



Transplantation of human embryonic stem cell-derived retinal pigment epithelial cells via injectable microfluidic-templated microgels for retinal regeneration

Ying Wei^{a,1}, Cong Ma^{a,1}, Chuanfeng An^{b,c}, Yujie Zhang^{b,c}, Haoyue Zhang^{b,c}, Qiyou Li^d, Li Kong^e, Huanan Wang^{b,c,*}, Xiang Ma^{a,**}

^a Department of Ophthalmology, The First Affiliated Hospital of Dalian Medical University, Dalian, 116014, China

^b MOE Key Laboratory of Bio-Intelligent Manufacturing, Dalian Key Laboratory of Artificial Organ and Regenerative Medicine, School of Bioengineering, Dalian University of Technology, Dalian, 116024, China

^c State Key Laboratory of Fine Chemicals, Frontiers Science Center for Smart Materials Oriented Chemical Engineering, Dalian University of Technology, Dalian, 116024, China

^d Southwest Hospital/Southwest Eye Hospital, Third Military Medical University, Chongqing, 400038, China

^e Department of Histoembryology, Dalian Medical University, Dalian, 116044, China

ARTICLE INFO

Keywords:

Cell-laden microgel
Microfluidics
Injectable granular gel
hESC-RPE
Cell transplantation

ABSTRACT

Retinal pigment epithelial (RPE) cells are specialized neural cells crucial for vision, while human embryonic stem cell-derived retinal pigment epithelial (hESC-RPE) cells hold great potential as a viable cell source for treating retinal degenerative diseases like retinitis pigmentosa (RP). However, the transplantation efficiency and viability of hESC-RPE cell suspensions are relatively low due to detrimental shear-force during operations and host immune-clearance. We herein develop an alternative transplantation strategy with the aid of a microfluidic-templating microgel cell carrier to achieve substantially enhanced loading and delivery efficiency of hESC-RPE cells, thereby promoting visual function recovery after subretinal injection in the RP model Royal College of Surgeons (RCS) rats. Specifically, injectable monodispersed microgels consisting of gelatin-methacryloyl/Hyaluronic acid-methacryloyl core coated with fibrin shell (denoted as Fib@GHMS) were fabricated in a high-throughput and controllable manner, facilitating the adhesion and proliferation of hESC-RPE cells. RCS rats treated with microcarriers showed significantly improved visual function, evidenced by increased B-wave amplitudes and the preservation of the inner nuclear layer at 8 weeks post-surgery. In conclusion, our innovative delivery system Fib@GHMS for hESC-RPE cell transplantation presents a potential therapeutic graft for retinal tissue engineering. It may open a new avenue for clinical transplantation of minimally invasive cell-based treatments in retinal degenerative diseases.

1. Introduction

Retinal homeostasis depends on the functionality of retinal pigment epithelium (RPE) cells. Dysfunction in these cells can result in the secondary degeneration of retinal photoreceptor cells, ultimately leading to retinal degenerative diseases such as retinitis pigmentosa (RP) [1,2]. RP affects one in around 3000–4500 individuals, with over 2 million people affected worldwide [3]. It is a prevalent hereditary retinal disease that

causes progressive vision loss, night blindness, progressive visual field defects, retinal osteocyte-like pigmentation, wax-yellow atrophy of the optic disc, and physiological abnormalities [4]. The pathogenesis of RP often involves the degeneration and progressive atrophy of RPE cells, which disrupts the nutrient supply to the retina. Gene mutations impair the ability of RPE cells to bind and phagocytose the discs shed by photoreceptor outer segments [5]. This disruption hinders the normal metabolism of retinal photoreceptor cells, accelerates their apoptosis,

* Corresponding author. MOE Key Laboratory of Bio-Intelligent Manufacturing, Dalian Key Laboratory of Artificial Organ and Regenerative Medicine, School of Bioengineering, Dalian University of Technology, Dalian, 116024, China.

** Corresponding author.

E-mail addresses: huananwang@dlut.edu.cn (H. Wang), xma9467@vip.sina.com (X. Ma).

¹ Ying Wei and Cong Ma contributed equally to this work.

<https://doi.org/10.1016/j.mtbio.2025.101880>

Received 24 October 2024; Received in revised form 13 May 2025; Accepted 17 May 2025

Available online 23 May 2025

2590-0064/© 2025 Published by Elsevier Ltd. This is an open access article under the CC BY-NC-ND license (<http://creativecommons.org/licenses/by-nc-nd/4.0/>).

and contributes to the onset of RP, resulting in the disappearance of the b-wave in the electroretinogram [6]. Patients may suffer from irreversible visual impairments from birth, ultimately leading to blindness in both eyes. Unfortunately, there is currently no effective treatment for RP. Cell therapy is considered one of the most promising therapeutic strategies, especially for advanced diseases [7].

Recently, stem/progenitor cell transplantation for tissue and functional reconstruction has garnered widespread attention in regenerative medicine. Stem/progenitor cells possess unlimited proliferation capacity and multipotent differentiation potential, which allow them to satisfy the quantity and variety of cells required for clinical treatment [8]. Human embryonic stem cell-derived RPE cells (hESC-RPE) have been used in RP clinical trials [9]. However, the transplantation efficiency and survival rate of hESC-RPE cells still need to be polished [10]. Currently, cell therapy for the retina typically involves the injection of cell suspensions to deliver donor cells to the target tissue [11]. Nevertheless, the direct transplantation of stem cells might not be effective in many cases [12]. First, direct injection of cells alone might compromise cell viability, most likely due to the detrimental shear stresses during injection and operations [13,15]. Second, the transplanted cells have a low retention time in the injection site and many of the cells might “leak” rapidly. This is mostly due to the low cohesiveness and adhesiveness of the transplanted cells before they can produce sufficient amount of ECM. Third, the host tissue might not provide sufficient physical and chemical cues to the transplanted cells to support and direct their proliferation and differentiation. The use of stem cell carriers fabricated from biocompatible materials is a promising strategy to address the above mentioned issues. Stem cell carriers could increase the viability of stem cells during injection [16]. Upon injection, stem cell carriers could provide temporary mechanical and physical support before the cells take over through ECM secretion. In addition, bioactive molecules can be incorporated into the stem cell carriers to direct stem cell fate and facilitate targeted tissue formation.

Some studies attempted to improve the survival rate and visual function of transplants by using polarized monolayers or intact RPE cell sheets [12]. However, RPE cell sheet transplantation requires complex and invasive surgical procedures, leading to significant postoperative trauma and associated complications. Also, due to their inherent rigidity, RPE scaffolds cannot precisely adapt to the surface of the local retina [14]. Only a few cell carriers can be transplanted into the subretinal space in a minimally invasive manner [17]. However, current research is limited to the ARPE-19 cells and has not been evaluated for visual function in model animals [18,19]. The complex induction and cultivation conditions of retinal stem cells pose challenges to further exploration of cell-laden microgel transplantation in the field of ophthalmology. Previously, we investigated four standard biocompatible and biodegradable hydrogels for hESC-RPE cell transplantation [20]. In comparison to gelatin methacryloyl (GelMA), hyaluronic acid (HA), and alginate gels, fibrin emerged as a strong candidate for a 3D scaffold, exhibiting enhanced cell adhesion, viability, photoreceptor indicators, as well as the secretion of growth factors and *in vivo* cell survival. Consequently, we selected fibrin as the coating material to facilitate stem cell proliferation and functional expression.

Hydrogels are highly preferred in cell transplantation due to their resemblance to ECM, little immune response, and adjustable chemical and mechanical characteristics [21]. There has been increasing interest in micrometer-sized microgels composed of hydrophilic polymer networks dispersed in water [22]. Their small dimensions enhance sensitivity to environmental stimuli and facilitate greater diffusion rates and distances, which could be utilized for cell transplantation and administered through minimally invasive injection, thereby minimizing intervention in complex surgeries, discomfort, infection risks, and treatment costs [23]. Microgels can be fabricated via non-invasive photopolymerization methods, such as GelMA and HAMA hydrogels, eliminating the need for specific water/oil phase crosslinking conditions and streamlining the manufacturing process [24]. Microgels have shown

promise in stem cell transplantation for osteoarthritis and myocardial infarction. In ophthalmology, the injectable microgel-based cell transplantation may reduce invasiveness and optimize local adaptation post-cell transplantation to improve cell survival. Furthermore, microgels could provide a more uniform and controlled dispersion of cells, which guarantees the enhanced delivery efficiency. Therefore, an aggregated microsphere strategy is crucial for RPE cell transplantation.

In this study, we employed microfluidic droplet fabrication technology and modified a single-channel chip to facilitate the dual cross-linking of GelMA and HAMA, resulting in the degradable production of GelMA/HAMA microgels (GHMS) by the free radical polymerization process. Fibrin was used to cover the surface of the microgels to attach hESC-RPE cells, creating the cell-laden Fib@GHMS complex. We thoroughly analyzed the microgels' microstructure and mechanical characteristics. We assessed the cell viability and proliferation of hESC-RPE on the microgel surface and performed bioinformatics analysis with RNA-Seq. The transplantation efficiency and biocompatibility of the cell-laden Fib@GHMS injected into the subretinal space of RP model RCS rats were evaluated with ERG, OCT, histopathology, and molecular biology techniques (Fig. 1). When Fib@GHMS was transplanted, it preserved the viability and function of hESC-RPE cells and showed well injectability and biocompatibility, thus providing a novel minimally invasive transplantation strategy for hESC-RPE cells by combining materials for the first time. This approach holds enormous potential in improving stem cell therapy for retinal diseases.

2. Materials and methods

2.1. Preparation and characterization of Fib@GHMS

2.1.1. Fabrication of microfluidic chip

A microfluidic chip composed of polydimethylsiloxane (PDMS; Momentive, USA) was fabricated via conventional soft lithography processes [25]. The photomask was designed and printed using computer-aided design software (Art Services Company, USA). SU-8 2050 photoresist (MicroChem, MA, USA) was spin-coated to a thickness of 50 μm to make a master mold, which was exposed to ultraviolet (UV) light using the photomask. PDMS and the curing agent (2-hydroxy-4-(2-hydroxyethoxy)-2-methylpropiophenone) were poured over the master mold at a volume ratio of 10:1 and allowed to cure overnight at 65 $^{\circ}\text{C}$. The PDMS mold was removed from the master, and the entrance and exit of the channels were obtained using a biopsy punch with a diameter of 1 mm. After oxygen plasma treatment, the PDMS mold was bonded to a glass slide and cured at 65 $^{\circ}\text{C}$ for 1 h. To impart hydrophobicity to their surface, the microchannels were injected with the commercial hydrophobic saltwater Aquapel® (PPG Industries, PA, USA), incubated at room temperature for approximately 60 s, flushed using pressurized nitrogen gas, and incubated at 60 $^{\circ}\text{C}$ for 2 h (Fig. S1). The microfluidic chip includes a 25 \times 25 μm flow-focusing structure, a water phase inlet, an oil phase inlet, and a collection port (Fig. 2D).

2.1.2. Preparation and characterization of hydrogel precursors

2.1.2.1. Synthesis of HAMA. Hyaluronic acid (10 g, 48 kDa; Huaxi Biology, China) was dissolved in 500 mL of deionized water, and 3.6 g of methacrylic anhydride (Sigma-Aldrich, China) was slowly added at 4 $^{\circ}\text{C}$, followed by 5 M NaOH. The mixture was stirred for 4 h, transferred to a dialysis bag (molecular weight cutoff 7500), dialyzed against deionized water, and freeze-dried to obtain HAMA[26,27].

2.1.2.2. Synthesis of GelMA. Gelatin (10 g; Sigma-Aldrich, China) was dissolved in 250 mL of deionized water, and added 0.78 g of methacrylic anhydride. The pH was adjusted to 9 using 5 M NaOH. The mixture was stirred for 4 h at 50 $^{\circ}\text{C}$, transferred to a dialysis bag (molecular weight

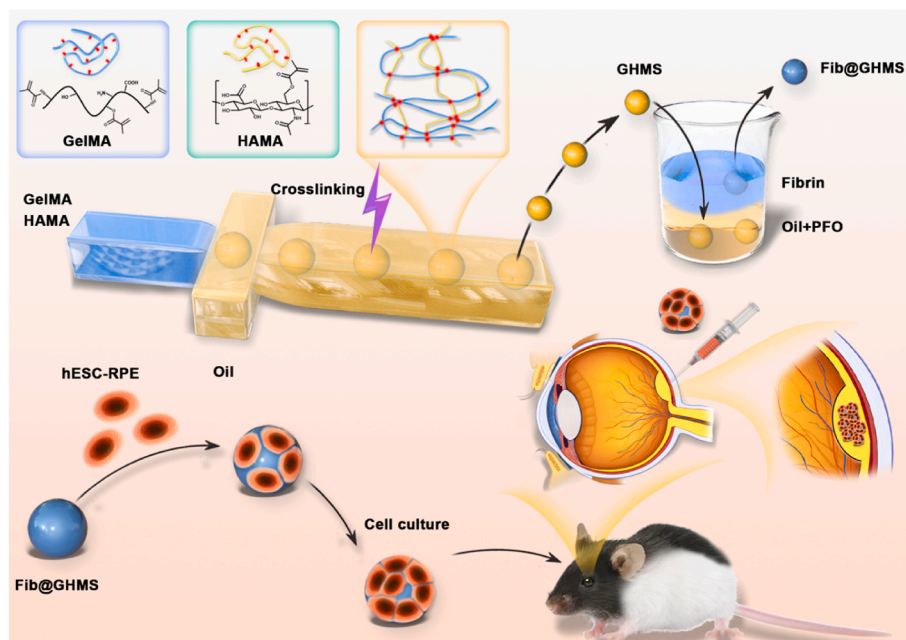


Fig. 1. Scheme showing the transplantation strategy using minimally invasive injection of hESC-RPE cell-loaded Fib@GHMS for the treatment of retinal degeneration diseases. Monodisperse GelMA/HAMA microgels (GHMS) were manufactured via microfluidic droplet-templating method followed by photopolymerization to solidify hydrogel precursor. Thereafter, the microgels were further coated with a thin layer of fibrin via immersing the microgels in aqueous solution containing fibrinogen, which were subsequently washed with thrombin to generate fibrin-coated GHMS (Fib@GHMS). hESC-RPE cells were cultured on the microgel surface *in vitro* to proliferate to a sufficient cell density, they were then injected into the subretinal space of RCS rats for transplantation.

cutoff 7500), dialyzed against deionized water for 3 days at 37 °C, and freeze-dried to obtain GelMA [28,29].

2.1.2.3. Preparation and parameter optimization of hydrogels. Different concentrations of GelMA and HAMA were explored for optimal degradation. The precursor solutions were prepared by dissolving 1 wt%, 2 wt%, or 3 wt% of GelMA, 0.2 wt% of lithium phenyl-2,4,6-trimethylbenzoylphosphinate (Sigma-Aldrich, China), and 0.1 wt%, 0.5 wt%, or 1 wt% of HAMA, in deionized water, denoted as G₁H_{0.1}, G₁H_{0.5}, G₁H₁, G₂H_{0.1}, G₂H_{0.5}, G₂H₁, G₃H_{0.1}, G₃H_{0.5}, and G₃H₁, respectively. The gelation procedure was chosen to facilitate the synthesis of bulk gels from the precursor solutions, to achieve gel formation at lower concentrations favorable for degradation. Images were captured using the Leica DM6000 microscope.

2.1.3. Microfluidic preparation of Fib@GHMS

All devices were wiped with 75 % alcohol and irradiated overnight with UV light before use. 1). The continuous phase: fluorinated oil (HFE7100, 3M, USA) with 0.5 wt% Krytox polyethylene glycol (PEG)-Krytox surfactant (DragonDrop, China), 1000 μL/h. The dispersed phase: G₂H_{0.5} gel precursor solution, 100 μL/h. Oil-encapsulated GelMA/HAMA cross-linked microgels (GHMS) were produced via droplet formation at 20 s⁻¹ and UV crosslinking at 360 nm for 15 s (Run LED, China) [30,31]. 2). Then, GHMS was added to a combination of 1H, 1H, 2H, 2H-perfluoro-1-octanol (PFO), and KnockOut DMEM with 0.5 % fibronectin (Sigma-Aldrich, China). The water-encapsulated microgel structure was generated overnight at 37 °C. 3). The second day, fibronectin-coated microgels were rinsed with PBS, resuspended in 10 U/mL thrombin (Sigma-Aldrich, China) at 37 °C for 5 min, and rewashed with PBS to obtain Fib@GHMS resuspended in the proliferation medium. Cryo-scanning electron microscopy (Quorum PP3000T microscope, UK) was used to characterize GHMS and Fib@GHMS.

2.1.4. Mechanical tests

The rheological properties of G₂H_{0.5} hydrogel precursor solution and Fib@GHMS particle gel were measured using the universal testing

machine (E43, MTS instrument, USA) with parallel plates having a 20-mm diameter at 37 °C. The linear viscoelastic range, which is the range in which a material exhibits linear behavior, was determined through frequency scanning. Shear-thinning behavior was characterized by a reduction in viscosity with increasing shear rate. The recovery percentage of G' before and after high-strain shear was measured to quantify the material's self-healing performance. PBS was added around the gel to hydrate the sample. Oscillatory time sweep tests were performed in the controlled-strain mode (0.5-mm gap and 1 Hz frequency) at 10 % strain for 60 s. The storage modulus (G', Pa) and loss modulus (G'', Pa) were determined in the initial time sweep. Frequency sweep oscillation tests were performed in the frequency range of 0.1–100 Hz (1 % strain). Strain (strain sweep) time sweep tests were conducted with a frequency range of 1 Hz (0.05–500 % strain, sampling interval of 10 points per 10-fold frequency).

2.1.5. In vitro degradation testing

Fib@GHMS samples were degraded at 37 °C using 0.5 U/mL type I collagenase and 0.5 U/mL hyaluronidase in PBS, flushed with deionized water at predetermined intervals to eliminate residual enzymes and freeze-dried again. The mass loss was calculated as follows:

$$\text{Degradation (\%)} = (M_1 - M_0) / M_1 \times 100$$

M₀ and M₁ represent the dry weight and initial weight of Fib@GHMS, respectively.

2.2. Proliferation and differentiation of hESC-RPE cells on the surface of Fib@GHMS

2.2.1. Cell microcarrier culture

As previously detailed, hESC-RPE cells were induced using the Q-CTS-hESC-2 cell line (Gibco, USA) and Essential 8 medium without exogenous sources. Briefly, to induce the spontaneous differentiation of hESC-RPE cells, hESCs were overgrown, spontaneously forming and acquiring RPE pigmented foci. The medium consisted of 77 wt% KnockOut DMEM, 20 wt% KnockOut Serum Replacement, 1 wt% CTS

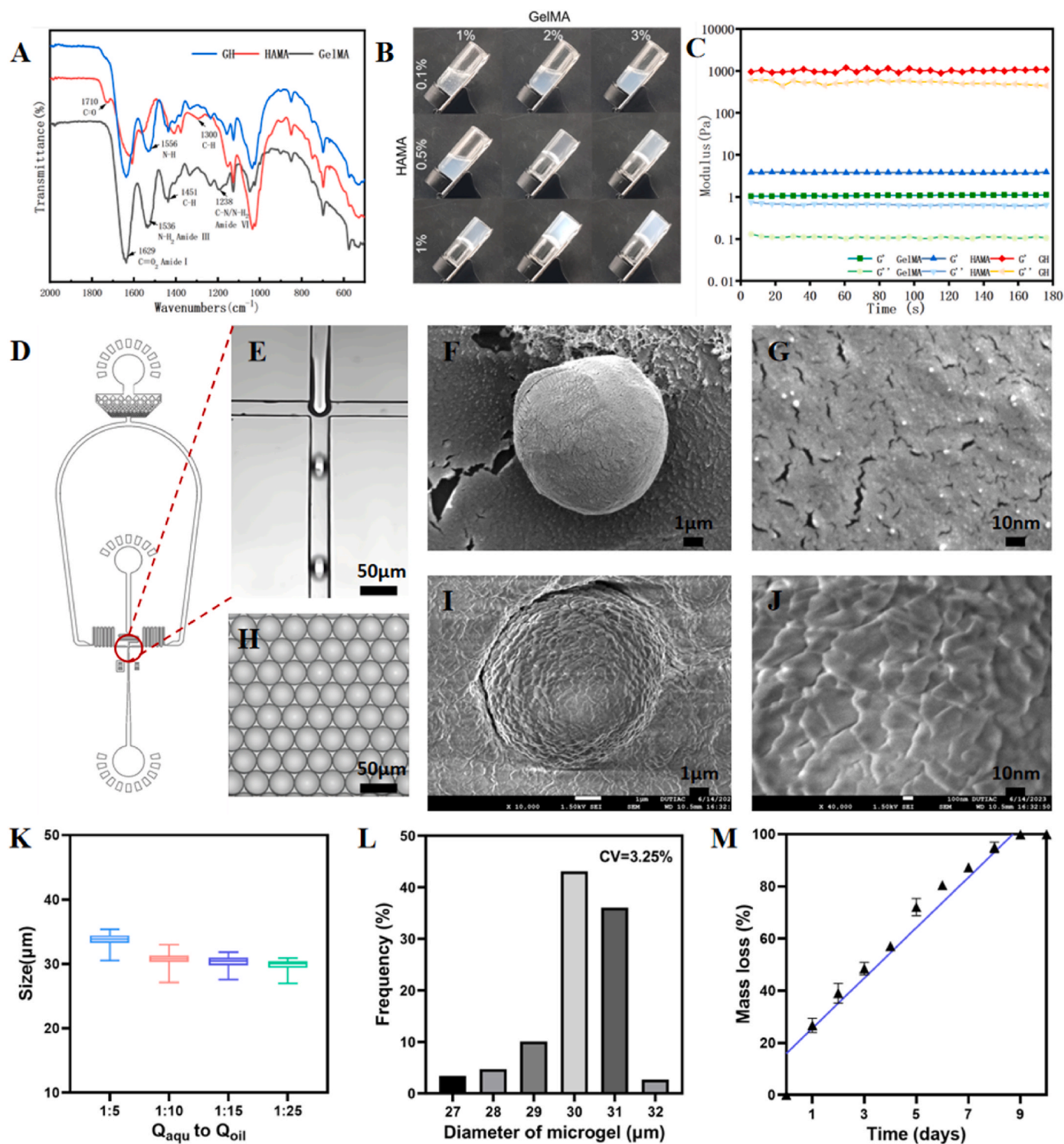


Fig. 2. Microfluidic-templating fabrication of Fib@GHMS microgels. **A:** FTIR spectra of HAMA, GelMA and composite GH hydrogels, showing the reduced peak at 1556 cm^{-1} corresponding to the GH double network hydrogel. **B:** Screening the minimum concentrations required of the GelMA and HAMA precursors to form a stable gel. **C:** Time sweeps of 2% GelMA, 0.5% HAMA, and $\text{G}_2\text{H}_{0.5}$ hydrogels to evaluate the mechanical performance. **D:** AutoCAD design of the microfluidic device. **E:** Microscopic images of the microchannel showing the preparation of uniformly sized aqueous droplets containing GelMA and HAMA precursors. **H:** Light microscopic images showing the generated monodisperse droplets. SEM images showing the morphology of GHMS (**F**, **G**) and Fib@GHMS microgels (**I**, **J**). **K:** The droplet size control via varying the flow ratio of $Q_{\text{aqu}}/Q_{\text{oil}}$. **L:** Statistical analysis of the microgel diameter range to analyze particle size uniformity. **M:** *In vitro* degradation of microgels.

GlutaMAX-I supplemented with L-glutamine, 1 wt% Minimum Essential Medium Non-Essential Amino Acids (Invitrogen, USA), and 1 wt% β -mercaptoethanol (Procell, China). hESC-RPE cells were incubated at $37\text{ }^\circ\text{C}$ in 5% $\text{CO}_2/95\text{ }\%$ air, and the medium was changed every 2 days.

The cells were isolated using CTSTM TrypLE™ Select Enzyme (Gibco, USA) and suspended in the medium before being seeded at a density of 1×10^5 cells/mL onto Fib@GHMS in 48-well plates[32,33]. To enhance the initial cell seeding density on the microsphere surface, we spread 0.1

mL of 1×10^3 /mL microspheres at the bottom of the plate, and then dropped 0.1 mL of 1×10^5 /mL cells onto the microspheres. Incubate the cells of high density at 37 °C for 4 h, then supplement the culture medium to 1 mL per well. Cells seeded at the same density on tissue culture polystyrene (TCP) served as the control.

2.2.2. Morphology, proliferation, and viability of hESC-RPE cells on Fib@GHMS

In order for rapid detection and minimal invasion, the LIVE/DEAD® Assay Kit (Invitrogen, Shanghai, China) was employed to measure the survival rate at 4 h, 1 day, 3 days, and 5 days. The cytoskeleton was observed by phalloidin staining (Thermo Fisher, USA, A22287) to verify the cell polarity and morphology. Fluorescent images were captured using an inverted fluorescence microscope and confocal laser-scanning microscope (OLYMPUS FV3000, Japan). Cell proliferation on Fib@GHMS was assessed by direct and sensitive DNA evaluation with the Quant-iT® dsDNA HS Assay Kit (Solarbio, China) every day for 6 days. Cell distribution on the microgel surface was evaluated every day for 5 days.

2.2.3. RNA-seq

To assess the impact of Fib@GHMS on the regeneration of hESC-RPE cells, cells grown on plates and microgels for 5 days were collected and sent to Majorbio (Shanghai, China) for RNA-seq. The RNA-seq libraries were generated using the standard Illumina TruSeq™ RNA Sample Preparation Kit on the Illumina HiSeq platform, following the manufacturer's instructions. Bioinformatic analysis was performed with Majorbio online platform[34,35].

2.2.4. Quantitative reverse transcription-PCR (qRT-PCR)

To explore the expression of vision-related genes in hESC-RPE cells grown on microcarriers, the cells were collected on day 5, and Fib@GHMS was dissolved using 10 U/mL type I collagenase and 10 U/mL hyaluronidase. Total RNA was extracted using the Omega Micro-Elute Total RNA Kit (Omega, USA), reverse-transcribed into cDNA using the PrimeScript™ RT Kit (Takara Bio, Dalian, China), and subjected to qRT-PCR using the Fast SYBR Green Master Mix (Applied Biosystems, USA) on the 7500 Fast Real-Time PCR System (Biosystems, USA). The sequences of the primers used are listed in Table S1 [36]. Gene expression was normalized to that of the housekeeping gene *GAPDH*, and the relative gene expression levels were calculated by the $2^{-\Delta\Delta CT}$ method.

2.2.5. Enzyme-linked immunosorbent assay (ELISA)

Cell detritus was eliminated by centrifuging the samples at 4 °C for 10 min at 2500 rpm, and the supernatants were stored at -80 °C for further analysis. The concentrations of vascular endothelial growth factor (VEGF) and pigment epithelium-derived factor (PEDF) were measured using VEGF and PEDF ELISA kits (Bosterbio, USA) on days 1, 2, 3, and 4, following the manufacturer's instructions.

2.2.6. Immunocytochemistry

hESC-RPE cells on the surface of Fib@GHMS were subjected to immunocytochemical analysis on day 5. The samples were fixed with 4 % paraformaldehyde at 4 °C for 20 min, probed overnight at 4 °C with primary antibodies (primary antibody details including concentration and cat # can be found in Table S2) in a solution of PBS containing 0.1 % Triton X-100 and 1 % bovine serum albumin, and incubated for 2 h at room temperature with Alexa Fluor 647-conjugated secondary antibodies (Invitrogen, USA) [37]. Cell nuclei were stained with 4',6-diamidino-2-phenylindole (Solarbio, China), and Fib@GHMS was labeled with fluorescein isothiocyanate. The samples were finally observed under the Leica DM IRB microscope (Leica Microsystems UK Ltd, Milton Keynes, UK).

2.3. Cell microcarrier implantation for restoring visual function in RCS rats

2.3.1. Cell microcarrier transplantation

All animal experiments followed the guidelines of the National Research Council's Guide for the Care and Use of Laboratory Animals and were approved by the Dalian University of Technology Animal Care and Use Committee (Approval No: DUTSBE230228-02). Sixty male P19 RCS rats weighing 50 ± 10 g each were obtained from the Army Medical University, Chongqing, China. They were individually housed at room temperature (25 ± 5 °C) and maintained on a 12-h light/dark cycle. Injections were administered into the subretinal cavity of the right eye of the rats, which were divided into four groups: the cell-loaded Fib@GHMS group, the cell group, the Fib@GHMS group, and the control group [38]. Rats were anesthetized by intraperitoneal injections of ketamine (93 mg/kg) and xylazine (8 mg/kg), and their pupils were dilated with tropicamide eye drops. An incision was made in the temporal aspect of the conjunctiva, and a 32-G needle was inserted 3 mm posterior to the corneal border and penetrated through the sclera. The cells were maintained at a low temperature throughout the operation. A microsyringe was employed to progressively introduce 2 μ L of liquid into the subretinal space via injection. The needle was maintained in position for 30 s prior to removal to reduce fluid leakage. Successful injections were confirmed by observing the spherical elevation on the retina through a glass coverslip. After surgery, all animals were administered water containing 210 mg/L cyclosporine and topical tobramycin/dexamethasone ocular ointment following surgery. Exclude rats with serious health problems and abnormal behavior.

2.3.2. Optical coherence tomography (OCT)

OCT was performed using a spectral domain OCT system ($n = 5$) (Bioptigen Inc., Durham, North Carolina). A volume analysis was performed with the optic nerve head as the focal point with 100 horizontal, raster, and continuous B-scan lines, each comprised of 1200 A-scans. The volume size measured 1.6 ± 1.6 mm. The biocompatibility and degradation of Fib@GHMS and the cells implanted into the subretinal space were assessed after 2, 4, and 8 weeks [39].

2.3.3. Electroretinography (ERG)

ERG was performed using the Espion E2 recording system ($n = 5$) (Diagnosys, Lowell, MA). After one night of dark adaption, RCS rats were anesthetized by intraperitoneal injections of xylazine (8 mg/kg) and ketamine (93 mg/kg). Their body temperature was maintained at 37 °C using a heating pad. After the pupils were dilated using local 2.5 % phenylephrine and 1.0 % tropicamide, corneal ERGs were recorded from both eyes using a gold wire loop and 2 % methylcellulose for corneal hydration. In addition to a ground electrode at the tail, the gold wire loops in the mouth served as the reference electrode. Our dark adaption ERG was conducted at $-2.31 \log \text{cd.s/m}^2$ to evoke rod-isolated responses. After adjusting the light for 10 min to a white backdrop with a contrast of 32 cd/m^2 , light adaption ERG was conducted at 1.09 $\log \text{cd.s/m}^2$. A total of 10–25 responses were recorded, with stimulation intervals varying from 3 to 60 s, depending on the strength of the stimulus. The B-wave amplitude, measured from the baseline to the peak of the waveform, was averaged for each response [40].

2.3.4. Histology and immunohistochemistry

To make retinal slices, the eyes ($n = 5$) were taken out, soaked in a 4 % paraformaldehyde solution for 3 h at room temperature, rinsed three times with PBS, soaked in PBS with 10 % and 20 % sucrose (Sigma LifeScience, S9378) for 2 h each, and then placed in a mix of optimal cutting temperature compound (Sakura, 4583) and 20 % sucrose. Continuous retinal/RPE/choroid sections were obtained with the cryostat, which was maintained at a low temperature. 6-mm-thick samples were stained with hematoxylin (Fisher Scientific, 3536-16) and eosin (Fisher Scientific, E511). Images were captured using the Leica DM6000

microscope. For immunohistochemistry, the sections were rinsed with PBS, treated for 1 h with 10 % goat serum (Sigma Life Science, G9023) and 0.1 % Triton X-100, probed overnight at 4 °C with anti-RPE65 (Abcam, ab231782) and anti-CRALBP (Abcam, ab15051), and incubated for 1 h at room temperature with secondary antibodies. Cell nuclei were stained using 4',6-diamidino-2-phenylindole [41].

2.4. Statistical analysis

Each sample was subjected to at least three experiments ($N \geq 3$), and the data were presented as the mean \pm standard deviation. Independent sample t-tests were employed for statistical comparisons, with statistical significance set at $P < 0.05$. Data analysis was performed using Image J and SPSS.

3. Results

3.1. Fabrication and characterization of cell microcarriers

Gelatin and hyaluronic acid are well-known biopolymers for applications in regenerative medicine regarding their excellent biocompatibility and biodegradability since they are the main components from native ECM [42,43]. Especially, hyaluronic acid is essential for preserving the functional organization of the retina and choroid [44]. Aiming to replicate the major composition of natural ECM, we herein chose to leverage the benefits of both gelatin and hyaluronic acid for the fabrication of a composite hydrogel matrix for better cell attachment and functionality. Moreover, considering the necessity to fabricate micrometer-sized carrier for cell attachment and feasibility of minimally invasive deliver [45], we herein prepared GelMA and HAMA for the generation of the composite hydrogel matrix. Our previous study showed that fibrous protein hydrogels supported the surface proliferation and functional expression of hESC-RPE cells better than GelMA and HAMA hydrogels, making them good carriers for hESC-RPEs. Taken together, to facilitate microfabrication and support cell adhesion and proliferation, we designed GelMA/HAMA composite hydrogel coated with fibrin protein as the delivery matrix for RPE cell (Fib@GHMS).

3.1.1. Microfluidic fabrication of GelMA/HAMA microgel carriers

To enable minimally invasive delivery of PRE cells for the treatment of retinal degeneration diseases, we proposed to fabricate spherical microgels as cell carriers, which can also enable the preparation of granular gels using the microgels as building blocks. GelMA and HAMA hydrogel precursors were synthesized following previously reported methods [30,46] and were chemically characterized by Fourier-transform infrared spectroscopy (Fig. 2A). The spectra confirmed the successful chemical functionalization of gelatin and HA and the formation of the double-crosslinked GelMA/HAMA hydrogel. Specifically, the characteristic peak at 1300 cm^{-1} corresponding to the vinyl CH of C=C bonds in HAMA was significantly attenuated after crosslinking, indicating the reaction of traditional photo-induced free radical polymerization of the methacrylate groups.

We explored the minimum concentration of each polymeric component required to form the stable hydrogel via the inversion method using the mixture of GelMA and HAMA precursors to facilitate cell delivery and accelerate *in vivo* degradation [47]. (Fig. 2B). It was found that 0.5 wt% HAMA and 2 wt% GelMA was sufficient for low-concentration gelation to produce a composite hydrogel (denoted as $G_2H_{0.5}$).

The mechanical properties of ECM can significantly regulate cell morphology and behavior. Therefore, we assessed the mechanical properties of the composite $G_2H_{0.5}$ gels using rheological measurement [27]. 2 wt% GelMA was a rather weak hydrogel with the storage modulus $G' = 1.1 \pm 0.1 \text{ Pa}$ by oscillatory time sweeps (10 % strain, 1 Hz). Meanwhile, 0.5 wt% HAMA showed similar $G' = 3.8 \pm 0.1 \text{ Pa}$ with GelMA. In comparison, the $G_2H_{0.5}$ hydrogels presented three order of

magnitude higher $G' = 1034.2 \pm 87.2 \text{ Pa}$ than single component. Increasing Mw and oxygen inhibition could potentially increase mechanical performance of the resulting hydrogel [30](Fig. 2C). Previous studies have reported that the retina is a soft tissue with a modulus below 1 kPa, suggesting that the low-concentration $G_2H_{0.5}$ hydrogel is suitable as an RPE transplant carrier for subretinal delivery [48].

For the generation of microcarriers for cell delivery, we employed a classic single-channel PDMS microfluidic chip (Fig. 2D and E) to generate stable oil-in-water emulsion droplets [49]. The droplets containing GelMA and HAMA hydrogel precursors were further initiated to gelate via UV light, thereby resulting in the formation of GelMA/HAMA spherical microgels (denoted as GHM) (Fig. 2H). The microfluidics technique allowed to generate microgels with high monodispersity and controllable size distribution. The microgel particle size could be adjusted by changing the flow rate ratio. When Q_{aqu} was fixed at 100 $\mu\text{L/h}$, the average diameter of the microgels ranged from 33.8 ± 0.9 – $29.8 \pm 0.7 \mu\text{m}$ as the flow rate ratio varied from 1:5 to 1:25 (Fig. 2K). Moreover, at a flow rate ratio ($Q_{\text{aqu}}/Q_{\text{oil}}$) of 1:10, the coefficient of variation of the microgel size distribution was low at 3.25 % (Fig. 2L). Considering our specific applications, the microgels with an average diameter of about 30 μm not only meet the microscopic size requirements of a typical 32-G injection needle with a 0.11-mm inner diameter but also ensure a certain post-transplantation mobility, avoiding dense cell aggregation. In conclusion, uniformly sized GHM were successfully prepared using this microfluidic system.

3.1.2. Preparation and characterization of Fib@GHMS microgels

The obtained HG microgels were further dispersed in aqueous solution of 0.5 % fibrinogen overnight, followed by induced-gelation of fibrinogen with thrombin to generate fibrin-coated microgels (denoted as Fib@GHMS). Cryo-scanning electron microscopy revealed a porous and rough microstructure for both GHMS and Fib@GHMS. The rough surface of Fib@GHMS microgels may be beneficial for cell adhesion (Fig. 2F, G, I, J) [50]. The *in vitro* degradation rate of Fib@GHMS may be indicative of its *in vivo* degradation behavior. Degradation profiles of Fib@GHMS are given in Fig. 2Q which reveals linear degradation profiles. When immersed in a solution containing 0.5 U/mL type I collagenase and 0.5 U/mL hyaluronidase, Fib@GHMS was almost completely degraded after 9 days. Therefore, low-concentration Fib@GHMS is a suitable carrier for retinal cell transplants (Fig. 2M).

By utilizing the microgels as building blocks, a granular gel with interconnected particulate network can be developed, which can thereafter enable injection-based delivery [51]. Oscillatory frequency sweep tests demonstrated that the microgels could form solid-like granular gels, as evidenced by the high G' than G'' regardless of the frequency. This indicated a viscoelastic gel with a frequency-dependent shearing response (Fig. 3A). The granular gels exhibited a high yield strain of around 80 % in subsequent strain sweep tests, indicating strong cohesive interactions among microgel particles (Fig. 3B). Impressively, Fib@GHMS granular gels also demonstrated shear-thinning and self-healing behavior, illustrated by the reduction in viscosity upon increasing shear rate and the rapid recovery of network modulus following network disintegration (Fig. 3C and D).

We hypothesized that the unique viscoelastic characteristics of Fib@GHMS may be attributed to the high concentration of hydrogen bonds created by the HA chains inside tightly packed microgel particles. However, the granular gels may be preserved at the defect location and retain structural stability *in vivo* [30]. Injectable and moldable cellularized scaffolds with advantageous mechanical properties may be extruded using standard medical syringes and needles [52]. This process enables the prompt restoration of mechanical strength and structural integrity after injection. (Fig. 3E).

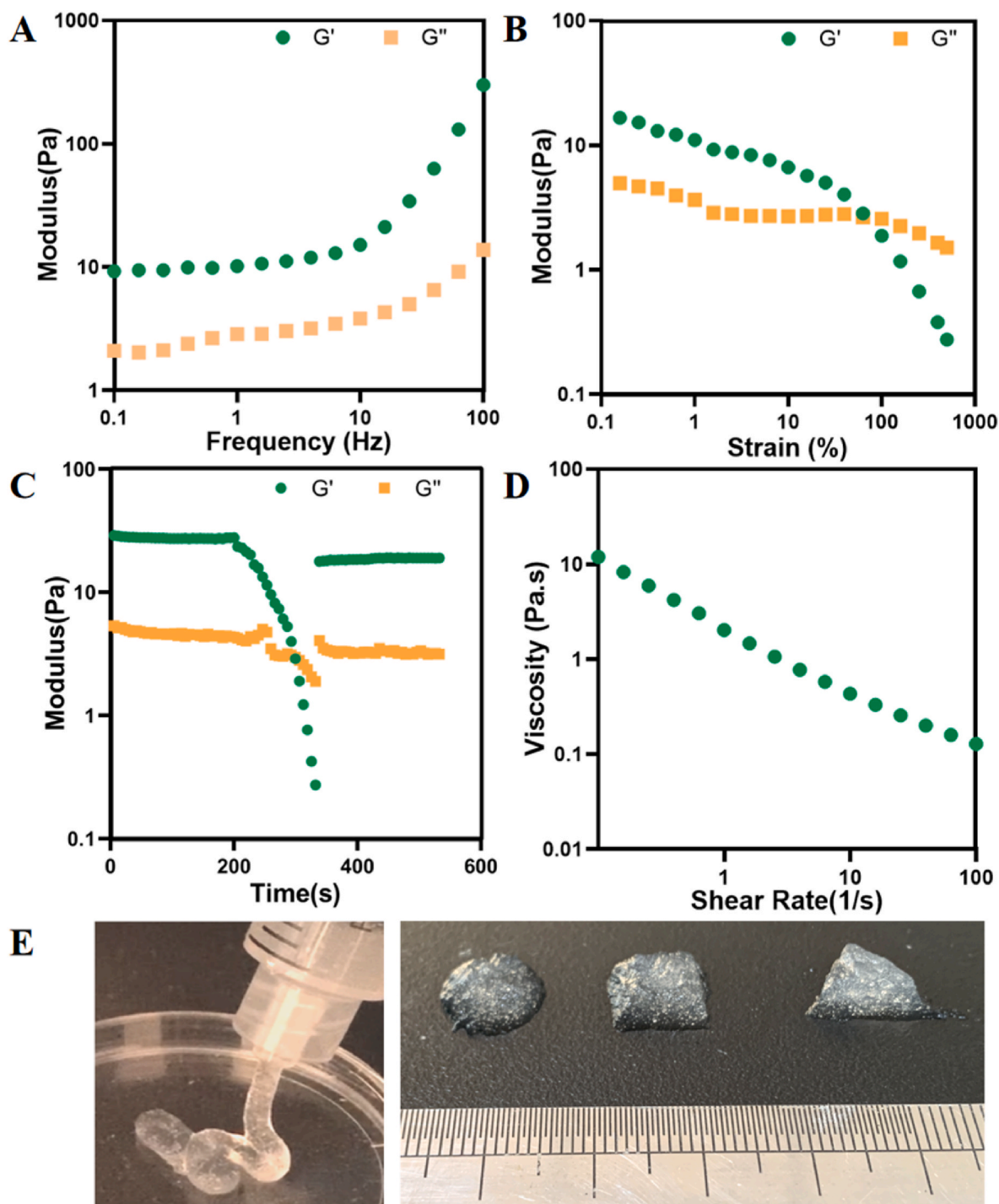


Fig. 3. Formulating shear-thinning, self-healing granular gels based on Fib@GHMS. A: Oscillatory frequency sweep (1 % strain) tests of granular gels of Fib@GHMS. B: Strain sweep (1 Hz) tests of Fib@GHMS. C: Evolution of Fib@GHMS storage and loss modulus during one destructive shearing cycle (strain from 0.5 % to 500 %, 1 Hz), showing granular gel self-healing. D: Granular gel viscosity as a function of shear rate revealed shear-thinning behaviour. E: Images of Fib@GHMS injectability and moldability.

3.2. Biological functional evaluation of hESC-RPE cells loaded on microcarriers

The biological functionality of hESC-RPE cells on Fib@GHMS microgels is crucial for practical applications and cell behavior studies at the single-cell level. Here, we assessed the biological functionality of hESC-RPE cells on the surface of microcarriers through cell attachment, proliferation, and functional expression assays.

3.2.1. Proliferation of hESC-RPE cells cultured on Fib@GHMS microgels

The viability and proliferation of hESC-RPE cells seeded on Fib@GHMS microgels were investigated, with cells seeded on TCP serving as the control. The viability of hESC-RPE cells was measured using the live/dead fluorescence assay after 4 h, 1 d, 3 d, and 5 d of culture. Most cells maintained alive with rare presence of dead cells when cultured on microcarriers (Fig. 4A). Quantitative analysis of cell distribution on the surfaces of microgels showed that most microcarriers initially contained single cells on their surfaces, but after 5 days, more

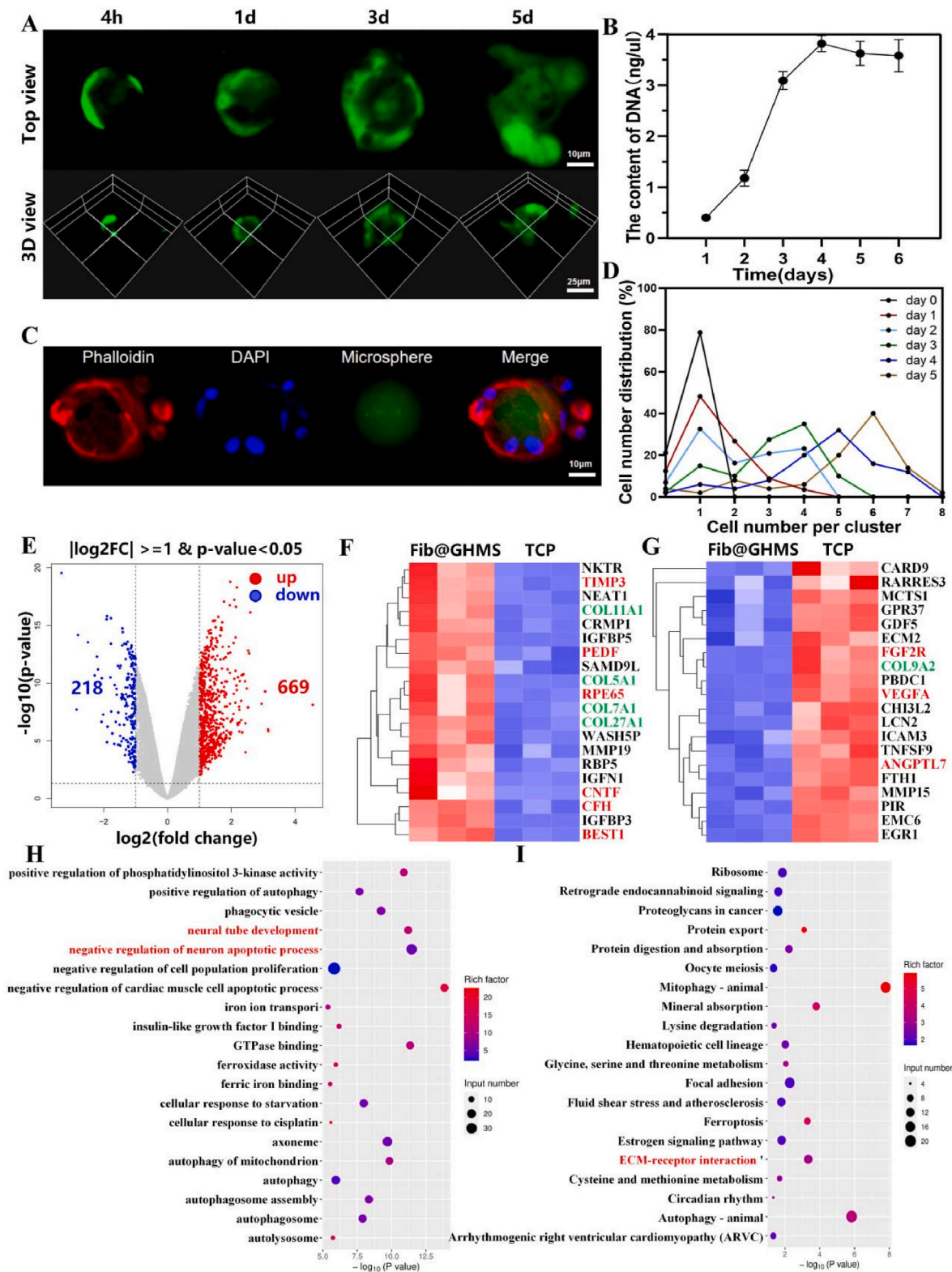


Fig. 4. The potential of hESC-RPE cell-Loaded Fib@GHMS microgels to restore retinal function. **A:** Cellular spreading and viability at different timepoints (4 h, 1 d, 3 d, 5 d) on the microcarriers. **B:** dsDNA cell proliferation assay of hESC-RPE cells cultured on the microcarriers. **C:** Cell cytoskeleton staining of hESC-RPE cells cultured on the microcarriers on day 5. **D:** Quantitative analysis of cell numbers on the microcarriers at different timepoints. **E:** Volcano plot depicting the DEGs between the Fib@GHMS and TCP groups. **F:** Heatmap of upregulated genes and **G:** downregulated genes in the Fib@GHMS group compared with the TCP group in the retinal function recovery microenvironment ($p < 0.05$). **H:** KEGG pathway enrichment analysis of DEGs. **H:** Twenty significantly enriched GO terms for the differential genes. **I:** Twenty significantly enriched KEGG pathways for the differential genes.

than 60 % of the microcarriers contained six or more cells (Fig. 4B). Cell cytoskeleton staining on day 5 revealed cells spreading on the microcarrier surfaces (Fig. 4C). Furthermore, DNA content determination demonstrated a rapid increase in cell proliferation, especially in the initial four days; the DNA content on day 4 was seven times higher than that on day 1, after which cell proliferation rate reached a plateau (Fig. 4D). We suggest that Fib@GHMS microgels provide a spatially restricted yet physiologically relevant microenvironment that supports cell viability and proliferation. The limited surface area and deformability of the microgel carriers may be the limiting factors for cell growth. These results reflect the excellent biocompatibility of Fib@GHMS microgels. Generally, hESC-RPE cells cultured on Fib@GHMS exhibit excellent adhesion, viability, and proliferation, thus underscoring the potential of this platform as a functionally injectable cell microcarrier for treating RP.

3.2.2. RNA-seq

To further elucidate the potential of hESC-RPE cell-loaded Fib@GHMS microcarrier to restore retinal function, RNA-seq analysis was performed on freely dissociated cells collected from the Fib@GHMS group and the control TCP group after 48 h of culture (Bioproject Accession: PRJNA1055668). The volcano plot showed 887 significantly differentially expressed genes, of which 669 were upregulated and 218 were downregulated (>2-fold, $p < 0.05$; Fig. 4E). We investigated the impact of the Fib@GHMS, and the results of RNA-seq analysis indicated that this microstructure affected the expression of genes related to neurotrophin, angiogenesis, proliferation, migration, and ECM synthesis, all of which are associated with retinal function recovery. The differences in gene expression between the TCP and Fib@GHMS groups were depicted using heat maps (Fig. 4F and G). Cells in the Fib@GHMS group carried significant higher regenerative potential, as evidenced by the upregulation of neurotrophic genes related to visual function recovery (*PEDF*, *RPE65*, *CNTF*, *BEST1*), antiapoptotic genes (*NFκB1*), and survival- and proliferation-related genes (*MAPK3*). Some important ECM synthesis genes (*COL11A1*, *COL5A1*, *COL7A1*, *COL27A1*, *MMP19*) were also significantly upregulated, indicating the potential of Fib@GHMS to promote cell and ECM regeneration as well as collagen deposition. The downregulation of angiogenesis-related genes (*VEGFA*, *ANGPTL7*) and other proteins suggested a lower risk of complications, such as retinal neovascularization.

Furthermore, Gene Ontology (GO) analysis indicated that some key enriched signaling pathways, such as neural tube development and the negative regulation of neuron apoptotic processes related to the nourishment of the optic nerve (Fig. 4H). Additionally, the Kyoto Encyclopedia of Genes and Genomes (KEGG) analysis highlighted key enriched signaling pathways, specifically those associated with ECM-receptor interactions involving the synthesis of the ECM (Fig. 4I). These analysis implies that our Fib@GHMS cell delivery system based on a synthetic three-dimensional microscopic scaffold can offer an inherent biocompatible and physiologically relevant microenvironment to support hESC-RPE viability and activity with enhanced functional paracrine superior over more conventional 2D cell culture. This scaffold can facilitate the survival, proliferation, and migration of hESC-RPE cells, while downregulating neuron apoptosis, thus exhibiting tremendous potential to restore retinal function.

3.2.3. Specific functional expression of hESC-RPE cells on Fib@GHMS microgels

We characterized the signaling potential of hESC-RPE cells implanted on the surface of Fib@GHMS microgels using the traditional TCP monolayer culture as a control. Fourteen RPE-specific genes grouped into three categories were chosen to assess cell functionality: choroidal stability-secreted factors (*TIMP3*, *FASL*, *VEGF-A*), photoreceptor stability-secreted factors (*PEDF*, *CNTF*, *GAS6*, *FGF2*), and general RPE functional markers (*RPE65*, *CFH*, *MYRIP*, *LHX2*, *CXCL8*, *LOXL1*, *CCL2*) (Fig. 5A). qRT-PCR data indicated that *PEDF*, *RPE65*, *TIMP3*, and *CFH*

were upregulated, while *GAS6*, *FGF-2*, *LHX2*, *CXCL8*, *LOXL1*, and *CCL2* were downregulated in microgel-loaded cells compared with adherent culture cells. *CCL2*, a regulator of immune responses in RPE cells, is upregulated during AMD. Meanwhile, the reduced expression of *LOXL1* and *LHX2* suggests cellular health and maturity of the hESC-RPE cells loaded onto Fib@GHMS microgels. To supplement this molecular characterization, we employed ELISA to assess the levels of proteins secreted by hESC-RPE cells loaded on Fib@GHMS surfaces or in conventional TCP cultures. hESC-RPE cells on Fib@GHMS secreted similar amounts of VEGF as cells in TCP cultures (Fig. 5B), but they produced significantly higher amounts of PEDF (Fig. 5C), a neurotrophic factor that has demonstrated significant therapeutic potential in preventing retinal degeneration by inhibiting photoreceptor apoptosis. VEGF is associated with choroidal neovascularization, and the lack of a significant impact on VEGF expression in our cell microcarriers represents the anticipated phenotype, potentially preventing the occurrence of wet AMD and further death of photoreceptor cells.

hESC-RPE cells on Fib@GHMS microgels were further immunostained to detect key RPE functional markers. Cells on the microgels exhibited detectable expression of cellular retinaldehyde-binding protein and lecithin retinal acyltransferase, both crucial proteins in the visual cycle function of RPE cells. We also verified the expression of bestrophin-1, typically found on the basal side of the RPE monolayer and involved in regulating calcium ions. The presence of the classic 'web-like' tight junction protein Zonula occludens-1 indicated the formation of tight connections between cells on the Fib@GHMS microgels. As hESC-RPE reorganizes into a monolayer on the microcarrier surface, deposition and remodeling of the ECM seems to occur. The secretion of ECM components, including laminin and fibronectin, by RPE cells appeared to be simulated in hESC-RPE cells cultured on Fib@GHMS. Furthermore, we observed the expression of two RPE-specific proteins: MITF, which is crucial for the development and function of RPE cells [53], and RPE65, which is essential for maintaining visual function in the normal visual cycle (Fig. 5D) [54]. It needs to be pointed out that, to the best of our knowledge, there are so far no study has performed in-depth characterization of not only the proliferation but also the functional paracrine secretion of RPE cells on microgel-based carriers. Therefore, our *in vitro* experiments demonstrated the potential of Fib@GHMS microgels as a transplantation vehicle for hESC-RPE cells, and pave the way for further translational applications of RPE cell-laden microcarrier system for clinical trials, particularly in transplantation via minimally invasive subretinal injection for the treatment of AMD and related diseases.

3.3. Subretinal injections of hESC-RPE cell-Loaded Fib@GHMS to promote visual function recovery

We transplanted different groups of grafts into the subretinal space of RCS rats, which are model animals for retinal degeneration occurring due to defective RPE phagocytosis of photoreceptor outer segments, leading to photoreceptor degeneration and gradual loss [55]. Beneficial from the substantially small size and monodispersity of the Fib@GHMS microgels and the injectability and adaptability of the microgel-based granular gels, the particulate material can be injected and further confined to the subretinal space of the affected eye. We further employed electrophysiological, histological, and molecular biology methods to thoroughly assess the restorative effects of hESC-RPE cell-loaded Fib@GHMS on the neural layer of the retina, photoreceptor cells, and retinal function in the affected eye.

3.3.1. OCT

We utilized OCT imaging to evaluate the short-term *in vivo* degradation and biological stability of the grafts in different experimental groups (cell-loaded Fib@GHMS, N = 15; cell group, N = 15; Fib@GHMS group, N = 15; Ctrl group, N = 15). Within 2 weeks, rats in all the treated groups showed noticeable subretinal elevation without abnormal

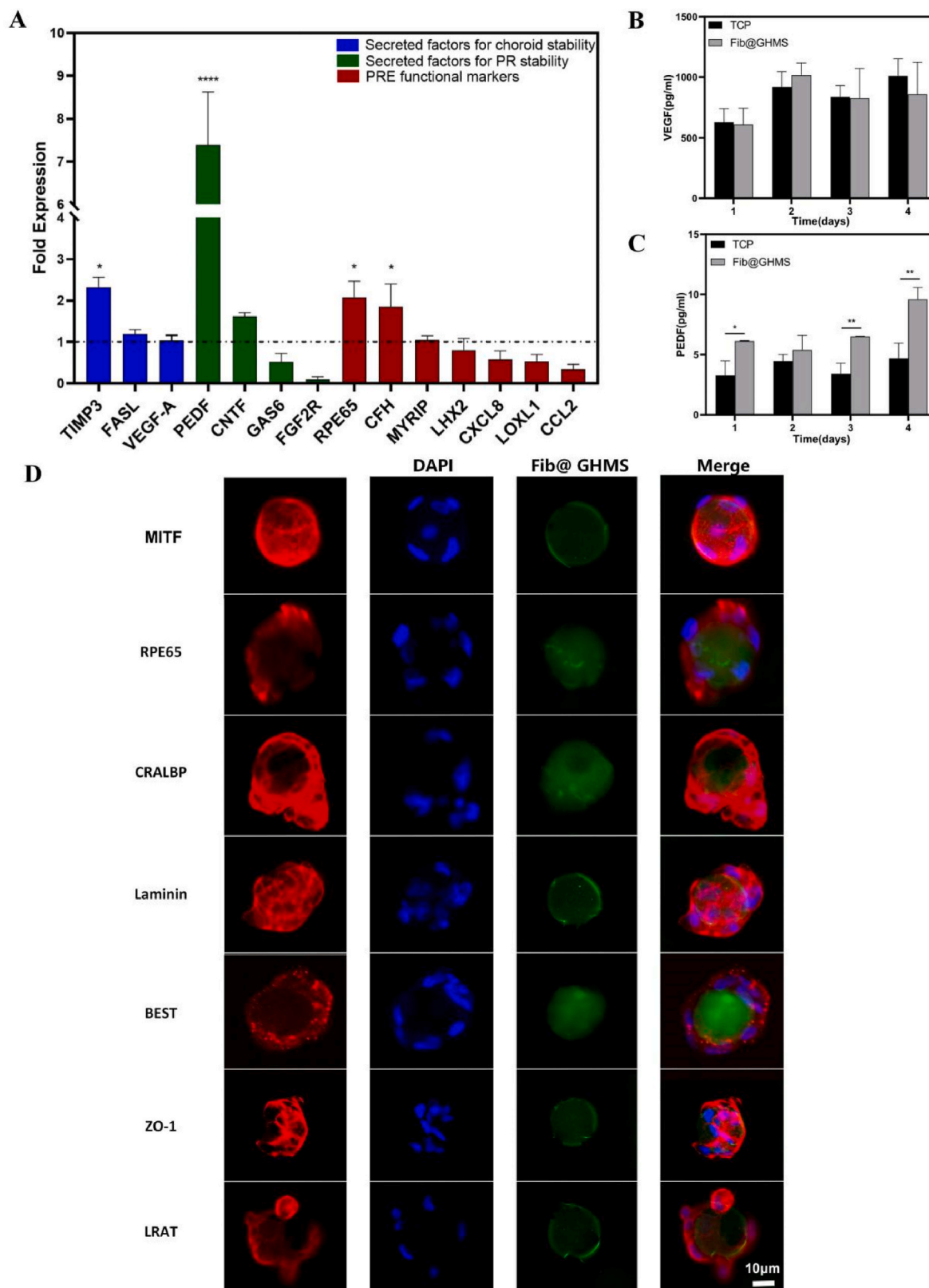


Fig. 5. Specific functional expression of hESC-RPE cells cultured on Fib@GHMS microgels. **A:** qRT-PCR comparing the expression profiles of key genes between hESC-RPE cells on Fib@GHMS and in TCP cultures (n = 3). The results are presented as 'fold expression' values to highlight the enhanced expression levels of certain genes in Fib@GHMS cultures compared with adherent cultures (dashed line). Gene expression was normalized to the endogenous reference gene (*GAPDH*). Wilcoxon paired signed-rank tests were used to compare ΔCt values for each gene in Fib@GHMS and adherent cultures. **B, C:** The levels of secreted PEDF and VEGF in conditioned culture media. The error bars represent standard deviations. **D:** Immunostaining of hESC-RPE cells on the surface of Fib@GHMS using antibodies against MITF, RPE65, CRALBP, Laminin, Best1, ZO-1, and LRAT. *p < 0.05, **p < 0.01, ****p < 0.0001.

structural changes in the retina. By 4 weeks, the transplanted materials no matter naked cells or cellularized microtissues (cells combined with microcarriers) in all groups had been partially degraded, with the cell-only group showing the most significant cell clustering. By 8 weeks, all the transplants in the different groups had completely degraded, and the inner nuclear layer of RCS rats remained generally intact, indicating the preservation of the activity of cells in this layer (e.g., Müller glial cells and amacrine cells) and the integrity of the inner limiting membrane (Fig. 6A). Compared with the untreated control group, the decrease in the retinal thickness after 8 weeks was lower in the cell-loaded Fib@GHMS group and the cells only group ($86.4 \pm 4 \mu\text{m}$ versus $62.8 \pm 4 \mu\text{m}$ and $68.5 \pm 3 \mu\text{m}$, respectively), suggesting that the function of transplanted cells to protect the retinal neuroepithelial layer maintained 8 weeks post-transplantation at least ($p = 0.004$ and 0.03 , respectively) (Fig. 6C) (summarized from Fig. 6A). This result was consistent with subsequent retinal histological findings. As the grafts grew in the subretinal space (the cavity between the neural retina and the RPE layer), the materials did not invade the retinal vessels due to the blood-retinal barrier. Moreover, their degradation products were nontoxic to the retina. Thus, after transplantation, Fib@GHMS loaded with cells do not cause retinal vascular occlusion or other retinal complications. Considering the excellent biocompatibility of microgels and their potential as cell delivery vehicles, they can be widely used in cell therapy and drug delivery systems. Using tissue engineering techniques, we developed hESC-RPE-loaded Fib@GHMS microtissues and successfully implanted them into the subretinal space of rats. These microtissues showed desirable biocompatibility, proper degradability, and the potential to provide a suitable microenvironment for RPE cell transplantation. However, further experiments need to be performed to validate their restorative effects on the neural layer of the retina, photoreceptor cells, and retinal function in the affected eye.

3.3.2. ERG

ERG was employed to evaluate electrophysiological function in model rats at various periods post-transplantation, with a-wave enhancement indicating photoreceptor functionality and b-wave typically reflecting bipolar cell activity (Fig. 6B). At 2 weeks post-transplantation, both amplitudes in the cell-loaded Fib@GHMS group were significantly elevated compared to the cell-only group, while showing no significant difference from the Fib@GHMS-only and sham groups, indicating that the transplantation of cell-loaded Fib@GHMS may positively affect visual function in a relatively short period. At 4 weeks post-transplantation, the a-wave exhibited no significant difference, whereas the b-wave was markedly elevated in the cell-loaded Fib@GHMS group compared to the cell-only groups. Both amplitudes were significantly higher in the group that had cells loaded with Fib@GHMS compared to the control group. This showed that Fib@GHMS has long-lasting protective effects on the function of hESC-RPE cells in preserving the retinal neuroepithelial layer. The 8-week ERG findings demonstrated that the amplitude was consistently larger in the cell-loaded Fib@GHMS group compared to the cell-only group. However, the disparity in amplitude between the two groups diminished. This indicates that the therapy attained a steady level with no further substantial rise (Fig. 6D and E). In conclusion, after 2, 4, and 8 weeks post-transplantation, ERG measurement revealed substantial enhancements in electrical activity, indicating that cell-loaded Fib@GHMS microcarriers have a prolonged therapeutic impact over an extended period. Our work shows that subretinal transplantation of hESC-RPE cell-laden Fib@GHMS might restore visual function in retinitis pigmentosa, hence strongly endorsing additional research and advancement of therapeutic strategies for retinal degenerative diseases.

3.3.3. Histological and histopathological analysis

Hematoxylin and eosin staining of rat retinas at 2 and 4 weeks post-transplantation revealed evident retinal bulging in the transplant area. In contrast, the bulge vanished and the retina returned to flattening at 8

weeks. No rosette-like formation [56] or other aberrant structures were present in the retina, nor was there a considerable degree of monocyte infiltration [57], indicating an absence of inflammatory reactions that substantially impacted the retinal structure (Fig. 7A). In addition, we provided *in vivo* degradation data of the transplantation area. We found that no matter which transplantation group, the subretinal space transplanted area had degraded, and the retina returned to the physiological flat state at 8 weeks (Fig. 7B). This conclusion aligns with the findings of OCT (Fig. 6A), indicating that after hESC-RPE cell-laden microcarrier transplantation, the grafts disseminate within the subretinal space under the pressure of the vitreous cavity, rather than forming the localized bulge. This phenomenon facilitates the development of subsequent single-layer RPE grafts, potentially attributable to the shear-thinning and self-healing behavior of Fib@GHMS (Fig. 3C and D). Further experiments are needed to determine the therapeutic effects of cell-loaded Fib@GHMS on retinal degeneration *in vivo*. As retinal degeneration progresses, the thinning of photoreceptor outer segments is accompanied by the thinning of the outer nuclear layer (ONL). In the advanced stages of the disease, photoreceptor outer segments and the ONL are entirely lost, while the inner nuclear layer is relatively well-preserved. Compared with the cell-loaded Fib@GHMS group, the ONL thickness from the optic disc's central and peripheral loci (3 mm diameter) from one representative eye of each group after 8 weeks was relatively low in the cell-only group, indicating that the anti-degenerative activity of transplanted cells was maintained for at least 8 weeks (Fig. 7C and D). The trend of hESC-RPE Cell-Loaded Fib@GHMS transplantation could also be illustrated in Fig. 7E, showing the rescue of the retina layer thickness from one representative eye of each group. This result was consistent with the previous retinal OCT findings. In the treated retinas, the area around the injection site displayed the most significant photoreceptor rescue, but photoreceptor rescue was also observed outside the injection area. The hESC-RPE cells were prelabeled with DiI, all RPE cells were labeled with RPE-specific 65 kDa protein, and the photoreceptor layer was labeled with cellular retinaldehyde-binding protein. Immunofluorescence results showed that Fib@GHMS was still present in the subretinal space at 4 weeks, whereas the cell-only group showed significantly fewer labeled cells around the transplantation site. At 8 weeks, the fluorescence had gradually decreased in the transplantation area, indicating that Fib@GHMS and some transplanted cells had degraded and been metabolized *in vivo* (Fig. 7F). Thus, cell-loaded Fib@GHMS treatment exhibited higher donor cell survival rates and transplantation efficiency compared with cell-only treatment, demonstrating a protective effect against retinal degeneration. This microcarrier system has the potential to serve as a biological material for retinal implants.

4. Discussion

Compared with traditional RPE cell-sheet delivery strategies [58], our work introduces a novel approach for RPE cell transplantation. We prepared Fib@GHMS microgels with uniform size via microfluidic droplet fabrication technology. Simultaneously, we focused on hESC-RPE cell transplantation and the Fib@GHMS microgels demonstrated superior performance in several aspects. Firstly, Fib@GHMS provided a larger surface area and biomimetic microenvironment, offering favorable conditions for the proliferation and specific functional expression of hESC-RPE cells. Furthermore, stem cell transplantation was greatly simplified and its complexity and risks reduced, thanks to the injectability, plasticity, and adaptability of Fib@GHMS, which required only minimal *in vitro* culture and minimally invasive surgery. Finally, we also validated its effectiveness in rescuing visual function in disease models.

In recent years, RPE cell transplantation has emerged as a cutting-edge strategy for the treatment of retinal diseases, with significant advancements achieved in research [60]. In conventional RPE cell transplantation methods, polarized monolayers or intact sheets of RPE cells

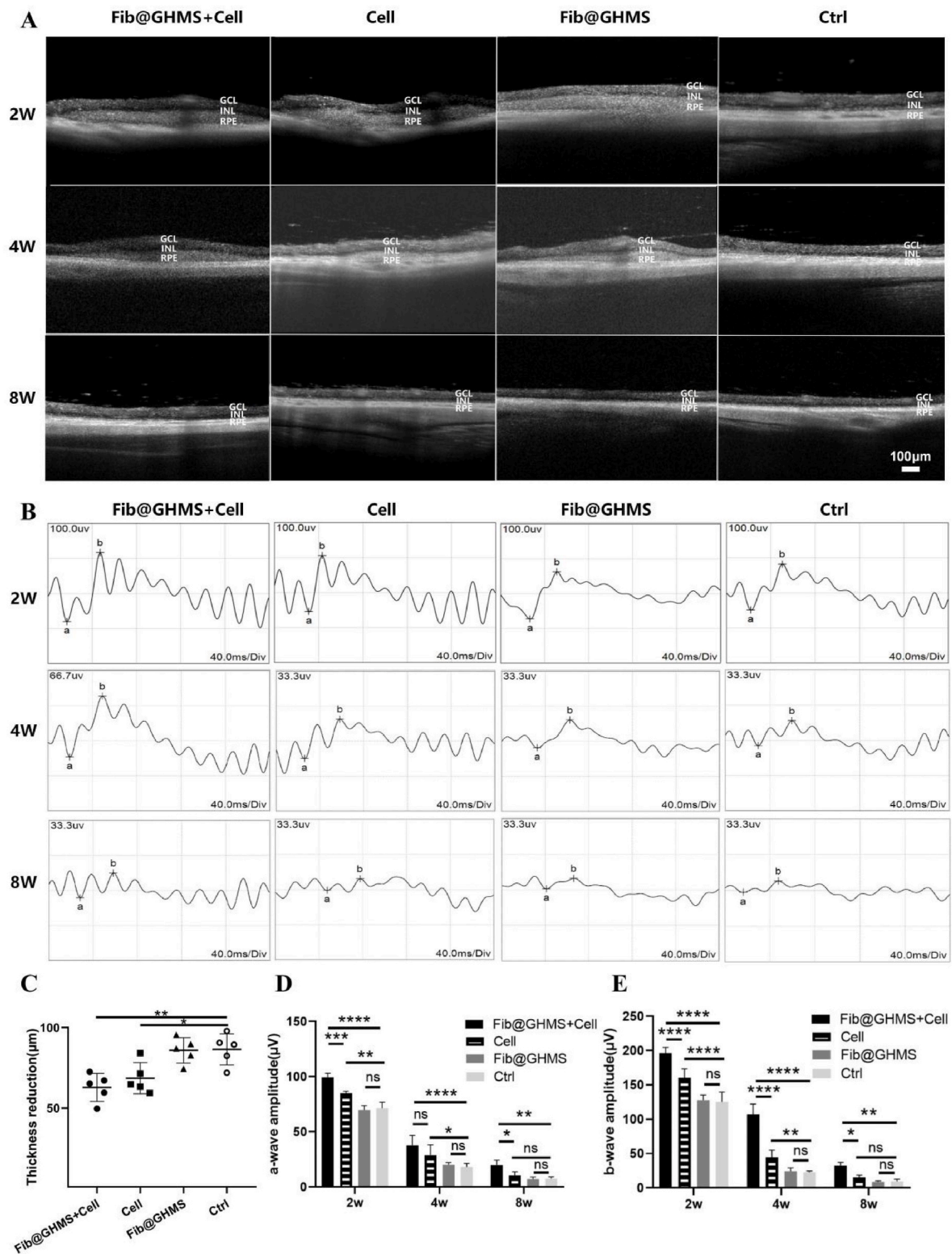


Fig. 6. Subretinal injection of hESC-RPE cell-loaded Fib@GHMS restores visual function. **A:** OCT evaluation of the biosafety and degradation status of hESC-RPE cell-loaded Fib@GHMS microcarrier in the subretinal space of RCS rats at 2, 4, and 8 weeks. Scale bar, 100 μm. GCL: ganglion cell layer; INL: inner nuclear layer; RPE: retinal pigment epithelium layer, including the transplanted RPE region. **B:** ERG assessment of the visual function recovery status of hESC-RPE cell-loaded Fib@GHMS in the subretinal space of RCS rats at 2, 4, and 8 weeks. **C:** Comparison of the relative decrease in retinal thickness (μm) in different groups at 8 weeks. **D:** Comparison of retinal a-wave and b-wave amplitudes (μV) for different groups at 2, 4, and 8 weeks. *p < 0.05, **p < 0.01, ****p < 0.0001.

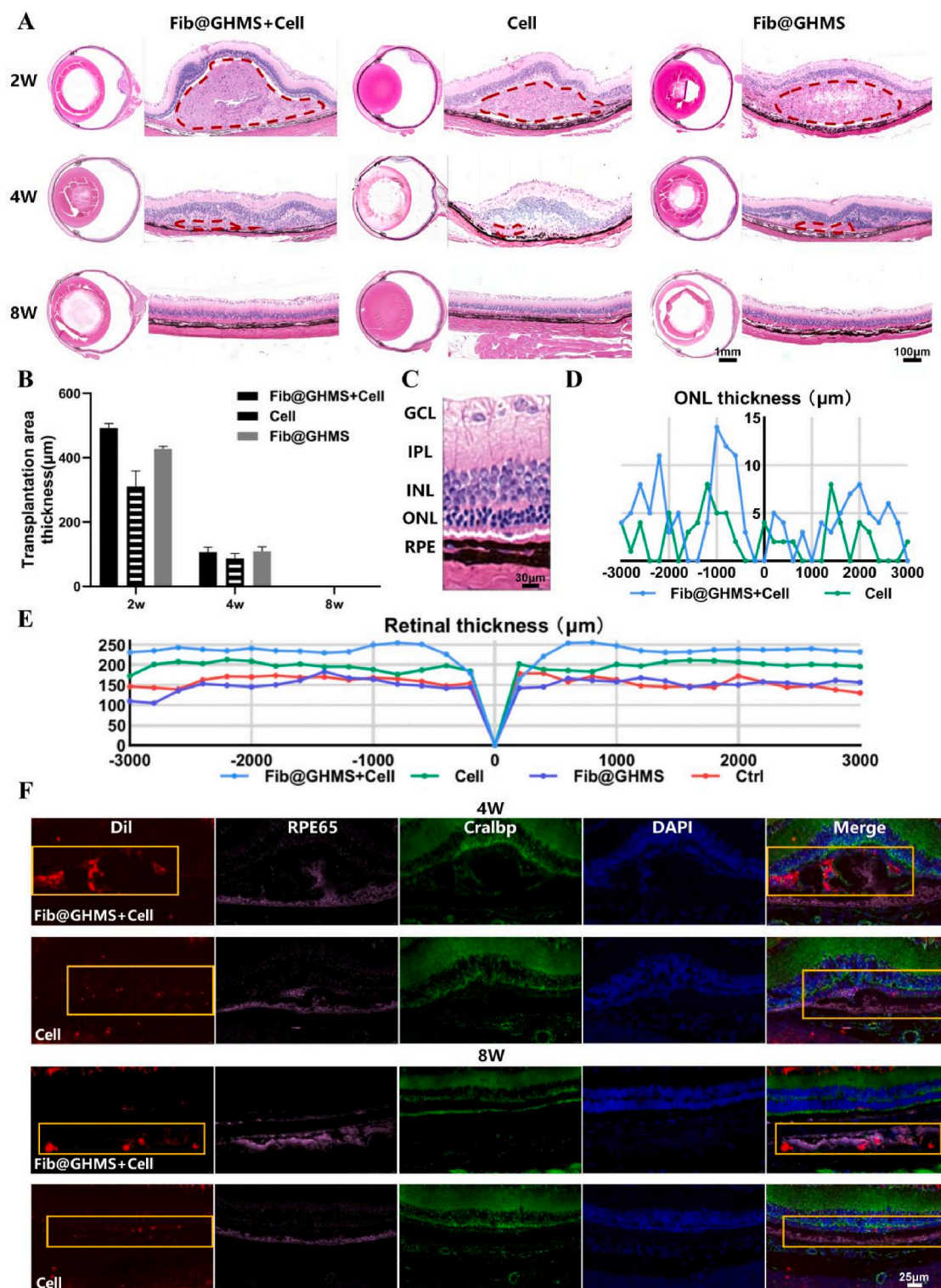


Fig. 7. Retinal morphological analysis and tissue immunofluorescence staining after hESC-RPE cell-loaded Fib@GHMS transplantation in RCS rats. **A:** Representative hematoxylin and eosin-stained images of the whole eye and the transplanted area of rats from each group at 2, 4, and 8 weeks. Observation of degradation in the transplanted area and assessment of graft biocompatibility. The red dashed area indicates the subretinal transplantation bulge region. **B:** Comparison of transplantation area thickness (μm) for different groups at 2, 4, and 8 weeks. **C:** Close up image of HE stained histological sections where the injection was administered, revealing the healthy retina. **D:** The horizontal thickness distributions of the ONL near the optic disc in RCS rats of each group at 8 weeks, summarized from the results of serial sections of eyes. **E:** The retina thickness at 8 weeks. **F:** Representative immunofluorescence images at 4 and 8 weeks. Evaluation of the short-term survival of transplanted cells and visual function recovery in RCS rats after the subretinal transplantation of Fib@GHMS and cells. Selected areas (orange box) were marked to further observe the grafted hESC-RPE. Red: Transplanted cells labeled with Dil; Pink: RPE65 staining to identify RPE cells; Green: Cralbp staining to identify RPE cells overlying photoreceptor cells; DAPI: Nuclear staining. (For interpretation of the references to colour in this figure legend, the reader is referred to the Web version of this article.)

have been used in attempts to enhance the survival rate and visual function of the grafts. However, these methods often require complex invasive surgical procedures, which not only increase the risk of post-operative trauma for patients but may also lead to severe complications [59]. Moreover, the transplant area experiences uncontrolled ectopic migration and backflow of cells, which reduces the total amount of transplanted cells and reduces the efficiency of transplantation. More importantly, transplanted cells from allogeneic sources face difficulties in forming suitable cellular polarity within the host's local pathological microenvironment and encounter challenges such as immune system clearance [8]. Against this background, genetically engineered cells may be encased in microspheres and implanted into the eye as microcapsules that secrete cell factors [61]. Furthermore, ARPE-19 cells were mixed with biodegradable PLLA: PLGA microspheres to investigate cell adherence and survival on their surfaces [18]. There have also been efforts to employ composite hydrogels with GelMA/chitosan microspheres as carriers for ARPE-19 cell transplants [19]. Despite the enormous therapeutic potential of hESC-RPE cells in repairing damaged retinas and improving vision, making them critical seed cells for cell transplantation, their growth conditions are more demanding than those of conventional cell lines. Cultivation of these cells requires specifically pre-treated substrates, and they struggle to survive in a non-attached state [19,62]. Consequently, there is a shortage of research explicitly addressing materials for hESC-RPE cell transplantation. To address this issue, we have developed a novel microgel carrier for RPE stem cell transplantation designed to support the adhesion, proliferation, and functional expression of these cells.

Transcriptome sequencing analysis of hESC-RPE cells cultured on microcarriers showed upregulation of light perception genes (RPE65, BEST1) and photoreceptor-nutrition genes (PEDF and CNTF), indicating cell maturity. Cell proliferation might be associated with high adhesion. Being cultivated on microcarriers may be the main reason for the fluctuations in RPE cell-specific molecular markers [63]. Longer cell culture on Fib@GHMS (>1 month) should be further tested to ensure that gene expression is not terminated permanently. PCR and ELISA tests confirm that hESC-RPE cell-laden microcarriers secrete several cytokines, including PEDF. PEDF is a 50-kD glycoprotein that may promote the accumulation and maturation of RPE pigment granules and the capacity of aging RPE cells to recover from oxidative stress by stabilizing the mitochondrial network [64]. In RP models, PEDF may be secreted to protect photoreceptors from oxidative stress-induced apoptosis by upregulating Bcl-2, suppressing Bax and Caspase-3, and preserving the integrity of the blood-retinal barrier [65]. Consequently, the release of PEDF by our hESC-RPE cell-laden microcarriers may be regarded as a potentially effective strategy for RP treatment.

Additionally, we evaluated the efficacy of this transplantation carrier in restoring visual functions in animal models. Nutritional assistance for photoreceptor cells indirectly enhances the amplitude of a-wave in ERG. Our findings indicated that the a-wave amplitude of ERG still considerably differs between the cell-loaded Fib@GHMS group and the cell-only group at 8 weeks post-transplantation, probably due to hESC-RPE cell-laden microcarriers can furnish photoreceptors with adequate nutritional support [66]. Additionally, the expression of retinal immunofluorescence RPE65 indicated that our microcarriers preserved retinal cycle, enhanced the survival and functional stability of hESC-RPE cells post-transplantation, and contributed to the improvement of visual recovery. However, single RPE cell transplantation was insufficient to restore visual function in RCS rats. The changes in the microenvironment need further confirmation.

While Fib@GHMS microgels show promise for stem cell transplantation treatment in treating RP by effectively addressing the drawbacks of the inadequate adhesion conditions that result in nonfunctional cell aggregates during cell suspension transplantation, as well as the complexities and traumas of monolayer cell scaffold transplantation, there are obstacles to overcome before practical use, including guaranteeing long-term cell survival and preventing immune response. We still

need to optimize the material preparation operations and ensure compliance with FDA standards to get clinical certification. Future research should focus on optimizing the design and function of microcarriers and enhancing therapeutic effects by adjusting the host microenvironment. At the same time, we could also employ gene modification to enhance the adaptability of stem cells in the pathological microenvironment, therefore improving transplantation efficiency. In summary, the development and application of the Fib@GHMS microcarrier system not only demonstrates significant progress in the field of RPE cell transplantation but also provides a safer and more effective new approach for the treatment of retinal degenerative diseases. These achievements will offer critical theoretical bases and technical support for future basic research and clinical practice.

5. Conclusion

The Fib@GHMS microgels, generated via microfluidic-templating technique in this study, offers not only superior properties over conventional cell sheet delivery strategy including larger surface area and biomimic microenvironment for hESC-RPE cells' proliferation and functionality, but also injectability, moldability and adaptability beneficial for the transplantation by requiring only a small-scale *in vitro* culture and minimally invasive procedures. Furthermore, hESC-RPE cells cultured on these microcarriers were provoked to secrete various cytokines, thereby providing additional nutritional support for the survival and maintenance of the transplanted cells as well as host photoreceptor cells. In general, this advancement allows for the use of stem cell transplantation in treating retinal degeneration diseases and highlights the crucial role of microcarriers in relative therapy approaches.

CRedit authorship contribution statement

Ying Wei: Writing – original draft, Software, Resources, Project administration, Methodology, Investigation, Formal analysis, Data curation, Conceptualization. **Cong Ma:** Supervision, Funding acquisition. **Chuanfeng An:** Methodology, Investigation, Formal analysis, Data curation, Conceptualization. **Yujie Zhang:** Software, Resources, Methodology, Investigation, Data curation. **Haoyue Zhang:** Methodology, Investigation, Data curation. **Qiyu Li:** Resources, Methodology. **Li Kong:** Methodology. **Huanan Wang:** Writing – review & editing, Visualization, Supervision, Funding acquisition, Conceptualization. **Xiang Ma:** Validation, Supervision, Resources, Funding acquisition.

Declaration of competing interest

The authors declare that they have no known competing financial interests or personal relationships that could have appeared to influence the work reported in this paper.

Acknowledgements

This work was supported by the National Key Research and Development Program of China (No. 2022YFC2403002), the National Natural Science Foundation of China (No. 81271022, No. 52273102).

All data included in this study are available upon request by contact with the corresponding author.

Appendix A. Supplementary data

Supplementary data to this article can be found online at <https://doi.org/10.1016/j.mtbio.2025.101880>.

Data availability

Data will be made available on request.

References

- [1] S. Yang, J. Zhou, D. Li, Functions and diseases of the retinal pigment epithelium, *Front. Pharmacol.* 12 (2021) 727870.
- [2] A. Lakkaraju, A. Umapathy, L.X. Tan, et al., The cell biology of the retinal pigment epithelium, *Prog. Retin. Eye Res.* (2020) 100846.
- [3] S.M. George, F. Lu, M. Rao, et al., The retinal pigment epithelium: development, injury responses, and regenerative potential in mammalian and non-mammalian systems, *Prog. Retin. Eye Res.* 85 (2021) 100969.
- [4] J.R. Sparrow, D. Hicks, C.P. Hamel, The retinal pigment epithelium in health and disease, *Curr. Mol. Med.* 10 (9) (2010) 802–823.
- [5] D. Intartaglia, G. Giamundo, I. Conte, Autophagy in the retinal pigment epithelium: a new vision and future challenges, *FEBS J.* 289 (22) (2021) 7199–7212.
- [6] W.C. Huang, P.K. Liu, N.K. Wang, Electroretinogram (ERG) to evaluate the retina in cases of retinitis pigmentosa (RP), *Methods Mol. Biol.* 2560 (2023) 111–122.
- [7] M. Zhou, J.S. Geathers, S.L. Grillo, et al., Role of epithelial-mesenchymal transition in retinal pigment epithelium dysfunction, *Front. Cell Dev. Biol.* 8 (2020) 501.
- [8] Y. Wang, D. Zhang, B. Shen, et al., Stem/progenitor cells and biodegradable scaffolds in the treatment of retinal degenerative diseases, *Curr. Stem Cell Res. Ther.* 13 (3) (2018) 160–173.
- [9] T.G. Qiu, Transplantation of human embryonic stem cell-derived retinal pigment epithelial cells (MA09-hRPE) in macular degeneration, *NPJ Regen. Med.* 4 (2019) 19.
- [10] S.D. Schwartz, J.P. Hubschman, G. Heilwell, et al., Embryonic stem cell trials for macular degeneration: a preliminary report, *Lancet (N. Am. Ed.)* 379 (9817) (2012) 713–720.
- [11] L. da Cruz, K. Fynes, O. Georgiadis, et al., Phase 1 clinical study of an embryonic stem cell-derived retinal pigment epithelium patch in age-related macular degeneration, *Nat. Biotechnol.* 36 (4) (2018) 328–337.
- [12] B.A. Aguado, W. Mulyasmita, J. Su, et al., Improving viability of stem cells during syringe needle flow through the design of hydrogel cell carriers, *Tissue Eng. PT A* 18 (7–8) (2012) 806–815.
- [13] E.M. Brydon, R. Bronstein, A. Buskin, et al., AAV-mediated gene augmentation therapy restores critical functions in mutant PRPF31+/- iPSC-derived RPE cells, *Mol Ther Methods Clin Dev* 15 (2019) 392–402.
- [14] L. Tichotová, H. Studenovská, G. Petrovski, et al., Advantages of nanofibrous membranes for culturing of primary RPE cells compared to commercial scaffolds, *Acta Ophthalmol.* 100 (5) (2021) e1172–e1185.
- [15] G.E. Salazar-Noratto, G. Luo, C. Denoëud, et al., Understanding and leveraging cell metabolism to enhance mesenchymal stem cell transplantation survival in tissue engineering and regenerative medicine applications, *Stem Cells* 38 (1) (2019) 22–33.
- [16] Z. Zhang, Injectable biomaterials for stem cell delivery and tissue regeneration, *Expert Opin. Biol. Ther.* 17 (1) (2017) 49–62.
- [17] L.M. Marquardt, S.C. Heilshorn, Design of injectable materials to improve stem cell transplantation, *Curr Stem Cell Rep* 2 (3) (2016) 207–220.
- [18] H.A. Thomson, A.J. Treharne, L.S. Backholer, et al., Biodegradable poly(α -hydroxy ester) blended microspheres as suitable carriers for retinal pigment epithelium cell transplantation, *J. Biomed. Mater. Res.* A 95 (4) (2010) 1233–1243.
- [19] X. Cheng, P. Yin, T. Li, et al., Injectable composite hydrogels encapsulating gelatin methacryloyl/chitosan microspheres as ARPE-19 cell transplantation carriers, *Biomater Sci-UK* 11 (1) (2022) 278–287.
- [20] Y. Wei, U. Alexandre, X. Ma, Hydrogels to support transplantation of human embryonic stem cell-derived retinal pigment epithelial cells, *Brain Sci.* 12 (12) (2022).
- [21] N. Mitrousis, A. Fokina, M. Shoichet, Biomaterials for cell transplantation, *Nat. Rev. Mater.* 3 (11) (2018) 441–456.
- [22] Y. Wang, L. Guo, S. Dong, et al., Microgels in biomaterials and nanomedicines, *Adv Colloid Interfac* 266 (2019) 1–20.
- [23] X. Liu, J. Tao, J. Liu, et al., 3D printing enabled customization of functional microgels, *ACS Appl Mater Inter* 11 (13) (2019) 12209–12215.
- [24] A. Blocki, F. Löper, N. Chirico, et al., Engineering of cell-laden gelatin-based microgels for cell delivery and immobilization in regenerative therapies, *Clin Hemorheol Micro* 67 (3–4) (2017) 251–259.
- [25] C. Chande, N. Riaz, V. Harbour, et al., Universal method for fabricating PDMS microfluidic device using SU8, 3D printing and soft lithography, *Technology* 8 (01n02) (2021) 50–57.
- [26] K. Yue, G. Trujillo-de Santiago, M.M. Alvarez, et al., Synthesis, properties, and biomedical applications of gelatin methacryloyl (GelMA) hydrogels, *Biomaterials* 73 (2015) 254–271.
- [27] Y. Fan, Z. Yue, E. Lucarelli, et al., Hybrid printing using cellulose nanocrystals reinforced GelMA/HAMA hydrogels for improved structural integration, *Adv Healthc Mater* 9 (24) (2020) e2001410.
- [28] B.H. Lee, N. Lum, L.Y. Seow, et al., Synthesis and characterization of types A and B gelatin methacryloyl for bioink applications, *Materials (Basel)* 9 (10) (2016).
- [29] K. Rahali, G. Ben Messaoud, C.J.F. Kahn, et al., Synthesis and characterization of nanofunctionalized gelatin methacrylate hydrogels, *Int. J. Mol. Sci.* 18 (12) (2017).
- [30] C. An, R. Zhou, H. Zhang, et al., Microfluidic-templated cell-laden microgels fabricated using phototriggered imine-crosslinking as injectable and adaptable granular gels for bone regeneration, *Acta Biomater.* 157 (2022) 91–107.
- [31] Q. Feng, D. Li, Q. Li, et al., Assembling microgels via dynamic cross-linking reaction improves printability, microporosity, tissue-adhesion, and self-healing of microgel bioink for extrusion bioprinting, *ACS APPL MATER INTER* 14 (13) (2022) 15653–15666.
- [32] S. Petrus-Reurer, P. Kumar, S. Padrell Sánchez, et al., Preclinical safety studies of human embryonic stem cell-derived retinal pigment epithelial cells for the treatment of age-related macular degeneration, *Stem Cells Transl. Med.* 9 (8) (2020) 936–953.
- [33] F. Michelet, A. Balasankar, N. Teo, et al., Rapid generation of purified human RPE from pluripotent stem cells using 2D cultures and lipoprotein uptake-based sorting, *Stem Cell Res. Ther.* 11 (1) (2020) 47.
- [34] S. Petrus-Reurer, A.R. Lederer, L. Bague-Vidal, et al., Molecular profiling of stem cell-derived retinal pigment epithelial cell differentiation established for clinical translation, *Stem Cell Rep.* 17 (6) (2022) 1458–1475.
- [35] B.H. Parikh, P. Blakeley, K. Regha, et al., Single-cell transcriptomics reveals maturation of transplanted stem cell-derived retinal pigment epithelial cells toward native state, *P Natl Acad Sci USA* 120 (26) (2023) e2214842120.
- [36] A. Al-Ani, S. Sunba, B. Hafeez, et al., In vitro maturation of retinal pigment epithelium is essential for maintaining high expression of key functional genes, *Int. J. Mol. Sci.* 21 (17) (2020).
- [37] A. Al-Ani, D. Toms, S. Sunba, et al., Scaffold-free retinal pigment epithelium microtissues exhibit increased release of PEDF, *Int. J. Mol. Sci.* 22 (21) (2021).
- [38] K.E. Kador, R.B. Montero, P. Venugopalan, et al., Tissue engineering the retinal ganglion cell nerve fiber layer, *Biomaterials* 34 (17) (2013) 4242–4250.
- [39] K. Adachi, S. Takahashi, K. Yamauchi, et al., Optical coherence tomography of retinal degeneration in royal College of Surgeons rats and its correlation with morphology and electroretinography, *PLoS One* 11 (9) (2016) e0162835.
- [40] M. Naser, S. Shushtarian, Amplitude and latency of electroretinographical peaks as a tool to predict the extent of retinal degeneration in retinitis pigmentosa patients, *J Ophthalmol Res* 3 (3) (2020).
- [41] M.E.I. Mohamed, E.A.A. El-Shaarawy, M.F. Youakim, et al., Aging changes in the retina of male albino rat: a histological, ultrastructural and immunohistochemical study, *Folia Morphol.* 78 (2) (2018) 237–258.
- [42] A. Mora-Boza, M. Puertas-Bartolomé, B. Vázquez-Lasa, et al., Contribution of bioactive hyaluronic acid and gelatin to regenerative medicine. Methodologies of gels preparation and advanced applications, *Eur. Polym. J.* 95 (2017) 11–26.
- [43] J.Y. Lai, D.H. Ma, Ocular biocompatibility of gelatin microcarriers functionalized with oxidized hyaluronic acid, *Mat Sci Eng C-Mater.* 72 (2016) 150–159.
- [44] M. Hemshekhar, R.M. Thushara, S. Chandranayaka, et al., Emerging roles of hyaluronic acid bioscaffolds in tissue engineering and regenerative medicine, *Int. J. Biol. Macromol.* 86 (2016) 917–928.
- [45] P.C. Dromel, D. Singh, E. Andres, et al., A bioinspired gelatin-hyaluronic acid-based hybrid interpenetrating network for the enhancement of retinal ganglion cells replacement therapy, *NPJ Regen. Med.* 6 (1) (2021) 85.
- [46] J. Youn, J.H. Choi, S. Lee, et al., Fabrication and evaluation of gellan gum/hyaluronic acid hydrogel for retinal tissue engineering biomaterial and the influence of substrate stress relaxation on retinal pigment epithelial cells, *Molecules* 27 (17) (2022).
- [47] I.M. Shaikh, S.L. Jadhav, K.R. Jadhav, et al., Aceclofenac organogels: in vitro and in vivo characterization, *Curr. Drug Deliv.* 6 (1) (2009) 1–7.
- [48] Y. Liu, R. Wang, T.I. Zarebinski, et al., The application of hyaluronic acid hydrogels to retinal progenitor cell transplantation, *Tissue Eng. PT A* 19 (1–2) (2012) 135–142.
- [49] N. Weigel, Y. Li, A. Fery, et al., From microfluidics to hierarchical hydrogel materials, *Curr Opin Colloid In.* (2022) 101673.
- [50] J. Brinkmann, H. Malyaran, M. Enezy-Ulbrich, et al., Assessment of fibrin-based hydrogels containing a fibrin-binding peptide to tune mechanical properties and cell responses, *Macromol. Mater. Eng.* (2023) 2200678.
- [51] M.H. Norahan, S.C. Pedroza-González, M.G. Sánchez-Salazar, et al., Structural and biological engineering of 3D hydrogels for wound healing, *Bioact. Mater.* 24 (2022) 197–235.
- [52] D. Li, K. Chen, H. Tang, et al., A logic-based diagnostic and therapeutic hydrogel with multistimuli responsiveness to orchestrate diabetic bone regeneration, *Adv. Mater.* 34 (11) (2022) e2108430.
- [53] J.L. Liao, J. Yu, K. Huang, et al., Molecular signature of primary retinal pigment epithelium and stem-cell-derived RPE cells, *Hum. Mol. Genet.* 19 (21) (2010) 4229–4238.
- [54] C.P. Hamel, E. Tsilou, B.A. Pfeffer, et al., Molecular cloning and expression of RPE65, a novel retinal pigment epithelium-specific microsomal protein that is post-transcriptionally regulated in vitro, *J. Biol. Chem.* 268 (21) (1993) 15751–15757.
- [55] L. Ru, N. Wu, K. Wei, et al., Improving cell survival and engraftment in vivo via layer-by-layer nanocoating of hESC-derived RPE cells, *Stem Cell Res. Ther.* 11 (1) (2020) 495.
- [56] M. Ishikura, Y. Muraoka, Y. Hirami, et al., Adaptive optics optical coherence tomography analysis of induced pluripotent stem cell-derived retinal organoid transplantation in retinitis pigmentosa, *Cureus* 16 (7) (2023) e64962.
- [57] X. Yang, Q. Wang, F. Shao, et al., Cell volume regulation modulates macrophage-related inflammatory responses via JAK/STAT signaling pathways, *Acta Biomater.* 186 (2023) 286–299.
- [58] P.V. Algreve, L. Berglin, P. Gouras, et al., Transplantation of RPE in age-related macular degeneration: observations in disciform lesions and dry RPE atrophy, *Graef Arch Clin Exp.* 235 (3) (1997) 149–158.
- [59] S. Xiao, T. Zhao, J. Wang, et al., Gelatin methacrylate (GelMA)-Based hydrogels for cell transplantation: an effective strategy for tissue engineering, *Stem Cell Rev Rep* 15 (5) (2019) 664–679.
- [60] V. Klymenko, O.G. González Martínez, M. Zarbin, Recent progress in retinal pigment epithelium cell-based therapy for retinal disease, *Stem Cells Transl. Med.* (2024).
- [61] E. Santos, G. Orive, A. Calvo, et al., Optimization of 100 μ m alginate-poly-L-lysine-alginate capsules for intravitreal administration, *J Control Release* 158 (3) (2011) 443–450.

- [62] A. Sorkio, S. Haimi, V. Verdoold, et al., Poly(trimethylene carbonate) as an elastic biodegradable film for human embryonic stem cell-derived retinal pigment epithelial cells, *J. Tissue Eng. Regen. Med.* 11 (11) (2017) 3134–3144.
- [63] N.V. Strunnikova, A. Maminishkis, J.J. Barb, et al., Transcriptome analysis and molecular signature of human retinal pigment epithelium, *Hum. Mol. Genet.* 19 (12) (2010) 2468–2486.
- [64] Y. He, K.W. Leung, Y. Ren, et al., PEDF improves mitochondrial function in RPE cells during oxidative stress, *Invest Ophth Vis Sci* 55 (10) (2014) 6742–6755.
- [65] S.J. Lee, D.S. Duncan, F.D. Echevarria, et al., Pressure-induced alterations in PEDF and PEDF-R expression: implications for neuroprotective signaling in glaucoma, *J. Clin. Exp. Ophthalmol.* 6 (5) (2015).
- [66] A. Hernández-Pinto, F. Polato, P. Subramanian, et al., PEDF peptides promote photoreceptor survival in rd10 retina models, *Exp. Eye Res.* 184 (2019) 24–29.